Study of the Carbon-13 and Deuterium Kinetic Isotope Effects in the Cl and OH Reactions of CH_4 and CH_3Cl

Stig R. Sellevåg,*,† Gunnar Nyman,‡ and Claus J. Nielsen*,†

Department of Chemistry, University of Oslo, P.O. Box 1033 Blindern, N-0315 Oslo, Norway, and Department of Chemistry, Physical Chemistry, Göteborg University, S-41296 Göteborg, Sweden

Received: September 2, 2005; In Final Form: November 3, 2005

Relative rate experiments have been carried out for three isotopologues of chloromethane and their reactions with Cl atoms and OH radicals. The OH and Cl reaction rates of CH_2DCl and CHD_2Cl were measured by long-path FTIR spectroscopy relative to CH_3Cl at 298 ± 2 K and 1013 ± 10 hPa in purified air. The FTIR spectra were fitted using a nonlinear least squares spectral fitting method including measured high-resolution infrared spectra as references. The relative reaction rates defined by $\alpha = k_{light}/k_{heavy}$ were determined to be $k_{OH+CH3Cl}/k_{OH+CH2DCl} = 1.41 \pm 0.05$, $k_{OH+CH3Cl}/k_{OH+CHD2Cl} = 2.03 \pm 0.05$, $k_{Cl+CH3Cl}/k_{Cl+CH2DCl} = 1.42 \pm 0.04$, and $k_{Cl+CH3Cl}/k_{Cl+CHD2Cl} = 2.27 \pm 0.04$. The carbon-13 and deuterium kinetic isotope effects in the OH and Cl reactions of CH_3Cl were investigated further using variational transition state theory, and the results were compared to similar calculations performed for the CH_4 + OH/Cl reaction systems. The calculations show that the order of magnitude difference for the carbon-13 kinetic isotope effect in the OH reaction of CH_3Cl compared to CH_4 reported by Gola et al. (*Atmos. Chem. Phys.* **2005**, *5*, 2395) can be explained by the lower barrier to internal rotation of the OH radical in the transition state of the CH_4 + OH reaction than in the CH_3Cl + OH reaction. The deuterium kinetic isotope effects can be explained in terms of combined variational effects and tunneling.

1. Introduction

Chloromethane (CH_3Cl) is the most abundant atmospheric halocarbon with a burden of around 5 Tg and the only significant natural source of chlorine to the stratosphere.[1] According to the latest assessment report by the World Meteorological Organization, the global budget of CH_3Cl is very uncertain because the quantified sources can account for only about 3/4 of the emissions required to balance the known sinks.[2] However, abiotic conversion of chloride to chloromethane was demonstrated recently to occur readily in dead plant material and this source, not yet quantified, may amount to as much as 2.5 Tg yr^{-1} on a global scale.[3]

Stable isotope analysis is a potentially powerful tool in studying the atmospheric budget of CH_3Cl. We have recently reported the kinetic isotope effects (KIE) in the OH and Cl reactions of CH_3Cl, $^{13}CH_3Cl$, and CD_3Cl from relative rate measurements.[4] Another study published recently showed that the CH_3Cl formed by the abiotic methylation process is extremely depleted in ^{13}C,[5] and Keppler et al.[6] have presented results from isotopic mass balance calculations using these findings together with data existing in the literature. The calculations of Keppler and co-workers have provided strong support for the contention that abiotic methylation of chloride in plants and soil organic matter provides the bulk of CH_3Cl released to the atmosphere.

The ^{13}C KIE reported for the OH reaction with chloromethane was 1.059 ± 0.008[4], an order of magnitude larger than for the OH reaction with methane, 1.0039 ± 0.0004.[7] For comparison, the ^{13}C KIE in the Cl atom reactions with methane and chloromethane are comparable, being 1.058 ± 0.010[8] and 1.070 ± 0.010,[4] respectively.

Why is the fractionation factor in the OH reaction with chloromethane so different from that with methane? To address this question and to elucidate the mechanisms behind the observed kinetic isotope effects, we decided to carry out additional kinetic experiments with CH_2DCl and CHD_2Cl and model the reactions using variational transition state theory (VTST). None of the previous theoretical studies of the chloromethane reaction rates with Cl and OH have considered the kinetic isotope effects.[9−14] Although several theoretical studies have been carried out on the Cl and OH reactions of methane,[11,15−21] we have included VTST calculations of the CH_4 + Cl/OH reaction systems for benchmarking purposes.

2. Experimental and Computational Methods

2.1. Chemicals and Synthesis. CH_3Cl (>99.5%, Aldrich) was used as received without further purification. CH_2DCl and CHD_2Cl were synthesized from CH_2DOH (>98%, Cambridge Isotopes) and CHD_2OH (>98%, Cambridge Isotopes), respectively, according to the two-step procedure reported by Weiss et al.[22] In the first step, the alcohol (25 mmol, 1 mL) was added slowly to $POCl_3$ (55 mmol, 5 mL; >98%, Fluka) at room temperature under magnetic stirring and reflux for about 1 h during which some HCl was formed. The second step was carried out in a closed system connected to a vacuum line: the alcohol/$POCl_3$ solution was added slowly to PCl_5 (34 mmol, 7 g; >98%, Fluka) at room temperature under reflux and magnetic stirring. After complete mixing, the solution was heated slowly to boiling for about 1 h. The reactant gases, chloromethane and HCl, were passed through a saturated aqueous solution of NaOH

* Corresponding authors. E-mail: s.r.sellevag@kjemi.uio.no; claus.nielsen@kjemi.uio.no. Fax: +47 2285 5441. Tel: +47 2285 5680.
† University of Oslo.
‡ Göteborg University.

10.1021/jp0549778 CCC: $33.50
Published on Web 12/07/2005

in which HCl was absorbed while the chloromethane gas was first trapped at 195 K and subsequently transferred to an ampule at 77 K. The infrared spectra of CH_2DCl and CHD_2Cl showed no traces of H_2O, HCl, $POCl_3$, or the respective deuterated methanols, and their purities are estimated to be the same as those of the parent alcohols, that is, >98%.

2.2. Reference Spectra. Fourier transform infrared (FTIR) spectra with 0.02 cm^{-1} resolution were recorded with a Bruker IFS 120 FTIR instrument equipped with an InSb semiconductor detector, a KBr beam splitter, and a 4000−1800 cm^{-1} bandpass filter. To achieve an acceptable signal/noise ratio in the resultant spectra, we co-added 128 scans employing boxcar apodization of the interferograms. The partial pressures of the chloromethane isotopologues were in the range of 10−15 mbar, and the cell (17 cm, CaF_2 windows) was filled to 1013 hPa with nitrogen (Air Liquide, 99.998%). Figure S1 (Supporting Information) displays the obtained high-resolution FTIR spectra of CH_2DCl and CHD_2Cl in the 3200−2000 cm^{-1} region.

2.3. Relative Rate Experiments. The kinetic study was carried out by the relative rate method according to the procedure given by Gola et al.[4] Only brief details will therefore be given here. Assuming that the reactants react solely with the same radical and that none of the reactants are reformed in any side reactions, the relative rate coefficient, k_{rel}, is given according to the following expression

$$\ln\left\{\frac{[H]_0}{[H]_t}\right\} = \alpha \ln\left\{\frac{[D]_0}{[D]_t}\right\} \quad \alpha = \frac{k_H}{k_D} \tag{1}$$

where $[H]_0$, $[D]_0$, $[H]_t$, and $[D]_t$ are concentrations of isotopologues H and D at the start and at the time t, respectively, and k_H and k_D are rate coefficients. A plot of $\ln\{[H]_0/[H]_t\}$ versus $\ln\{[D]_0/[D]_t\}$ will thus give the relative reaction rate coefficient $\alpha = k_H/k_D$ as the slope. In the present experiments, H is CH_3Cl and D represents the heavier deuterium-substituted chloromethane isotopologues.

The experiments were carried out in a 250 L electropolished stainless steel smog chamber equipped with a White-type multiple reflection mirror system with a 120-m optical path length for rovibrationally resolved infrared spectroscopy. The infrared spectra were recorded at a nominal resolution of 0.125 cm^{-1} and Fourier transformed using boxcar apodization with a Bruker IFS 66v FTIR instrument equipped with an InSb detector. The reaction chamber was equipped with UV photolysis lamps mounted in a quartz tube inside the chamber, and all experiments were carried out in synthetic air (AGA 99.999%; CH_4, CO, and NO_x < 100 ppbv) at 298 ± 2 K and 1013 ± 10 hPa. Initial mixing ratios of the chloromethane isotopologues in the reaction chamber were 5−6 ppm.

Control experiments were performed to check for loss of chloromethane via photolysis, dark chemistry, and heterogeneous reactions in the reactor. The lifetime of chloromethane in the reaction chamber was investigated with purified air as the diluent and with the relevant radical precursor mixtures in purified air in experiments lasting from 8 to 15 h. The UV absorption cross section of chloromethane is less than 6×10^{-24} cm^2 $molecule^{-1}$ at wavelengths above 236 nm,[23] and, in accordance, no direct photolysis in the reactor was detected.

Hydroxyl radicals were generated by photolysis of O_3 in the presence of H_2 (99%; AGA). Ozone was produced from oxygen (99.995%; AGA) using a MK II Ozone generator from BOC, which has a conversion efficiency of approximately 5%, and collected in a trap filled with silica beads at 195 K. Typical mixing ratios of ozone and hydrogen were 5×10^2 ppm and 2×10^3 ppm, respectively. Photolysis of ozone was carried out at intervals of 10−15 min using a Philips TUV 30W lamp ($\lambda_{max} \approx 254$ nm).

Chlorine atoms were generated by photolysis of 20−25 ppm chlorine gas (99.8%; AGA) at intervals of 1−10 min employing a Philips TUV 30W lamp ($\lambda_{max} \approx 254$ nm). The use of this lamp was preferred because it will photolyze HC(O)Cl and CH_2ClOOH produced in the degradation of CH_3Cl, see later.

The experimental FTIR spectra were analyzed using a global nonlinear least squares spectral fitting procedure.[24] The spectral features used in the analyses were the C−H stretching bands in the 3200−2500 cm^{-1} region and the C−D stretching bands in the 2280−2150 cm^{-1} region. The spectral data for HCl, H_2O, CO, CO_2, N_2O, O_3, and CH_4 were taken from the HITRAN database.[25] For CH_3Cl, CH_2DCl, CHD_2Cl, and the overtone/combinations bands of O_3 (for which HITRAN does not yet provide all isotopic data), experimental high-resolution FTIR spectra were used.

The data from the independent experiments were analyzed according to eq 1 using a weighted least squares procedure, which includes uncertainties in both reactant concentrations.[26] The uncertainties in the reactant concentrations were taken as the standard deviations from the least-squares fitting of the experimental infrared spectra. If a dataset showed a y intercept significantly different from zero, then the experiment was discarded.

2.4. Electronic Structure Calculations. MP2,[27] CCSD,[28] and CCSD(T)[29] calculations were carried out with the Gaussian 03 program.[30] Unrestricted wave functions were used to describe open-shell systems and bond-breaking processes (a multiconfigurational approach is currently too time-consuming); singlet ground-state structures were calculated using a restricted wave function. The core electrons were kept frozen in the calculations. Dunning's correlation-consistent aug-cc-pVXZ (X = D, T) basis sets[31] were employed in all calculations. CCSD(T)/aug-cc-pVDZ and CCSD(T)/aug-cc-pVTZ single-point correlation energies were extrapolated toward the basis-set limit using the extrapolation scheme of Halkier et al.[32]

$$E_{XY}^{\infty} = \frac{X^3 E_X - Y^3 E_Y}{X^3 - Y^3} \tag{2}$$

where E_X is the correlation energy obtained with the highest cardinal number X, and E_Y is the correlation energy obtained with cardinal number Y equal to $X - 1$. The cardinal numbers of the aug-cc-pVDZ and aug-cc-pVTZ basis sets are 2 and 3, respectively. In the following, such calculations will be denoted CCSD(T)/EB with "EB" being short for extrapolated basis.

The minimum energy path (MEP) connecting reactants and products were computed at the MP2/aug-cc-pVDZ level of theory using the intrinsic reaction coordinate (IRC) method of Gonzales and Schlegel.[33] The IRC calculations were carried out in mass-weighted Cartesian coordinates using a step size of 0.02 $u^{1/2}$ bohr.

2.5. Calculations of Rate Coefficients. Calculations of rate coefficients were carried out using interpolated variational transition state theory by mapping (IVTST-M)[34] using the sparse grid of geometries, gradients, and Hessians from the ab initio IRC calculations as input (the ratio between gradients and Hessians was, in general, 3:1). The electronic energy of the MEP was corrected by the interpolated single-point energy method (ISPE)[35] using the extrapolated CCSD(T) energies computed at all stationary points plus one nonstationary point (chosen near

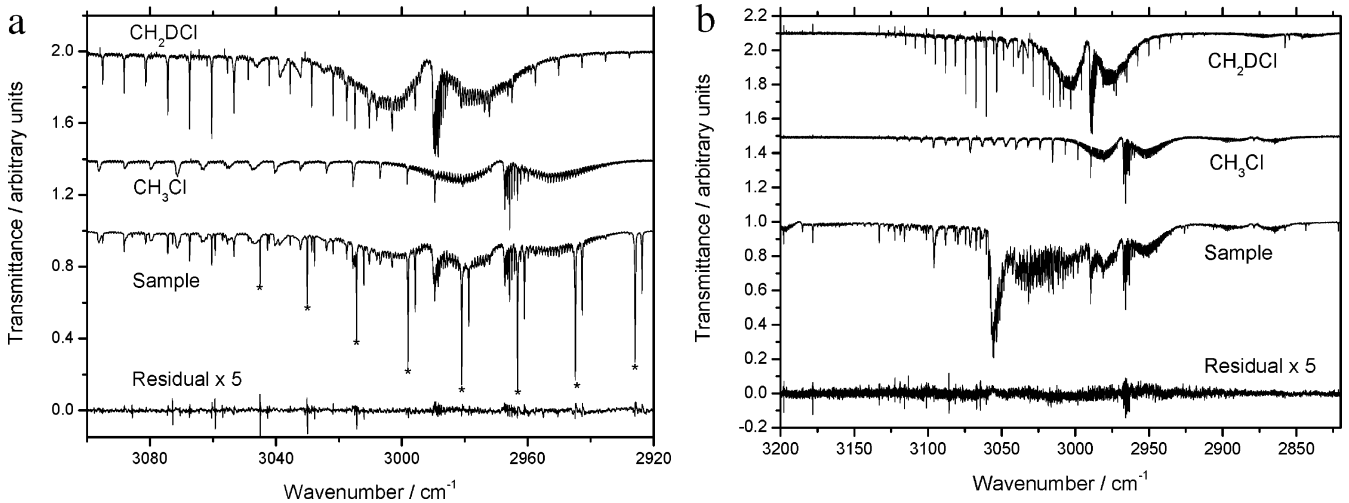

Figure 1. Experimental FTIR spectra of the reaction mixtures (a) $CH_3Cl/CH_2DCl/Cl_2$ after 30 min photolysis and (b) $CH_3Cl/CH_2DCl/O_3/H_2$ after 10 min photolysis. The two curves at the top are reference spectra of the chloromethane isotopologues (shifted for clarity). The bottom curve is the residual of the spectral fitting (magnified 5 times). The spectral lines marked with "*" belong to HCl. Compounds included in the spectral analysis of the Cl reaction experiments include CH_3Cl, CH_2DCl, H_2O, HCl, and CH_4. Compounds included in the spectral analysis of the OH reaction experiments include CH_3Cl, CH_2DCl O_3, H_2O, CH_4, and HCl.

the location of the dynamical bottleneck) as input. From this information, we obtained the ground state vibrationally adiabatic potential curve, V_a^G.

The rate coefficients were calculated over the temperature range of 200−1500 K using canonical variational theory (CVT)[36,37] and canonical unified statistical theory (CUS).[37,38] Semiclassical tunneling corrections have been included using the centrifugal-dominant small-curvature adiabatic ground-state tunneling (called small-curvature tunneling or SCT) approximation.[37,39] The transmission coefficient also includes the classical adiabatic ground-state (CAG) transmission coefficient,[40] that adjusts the quantal corrections for the difference between V_a^G at its maximum and at the CVT transition state. The calculation of the kinetic isotope effects were based on a single reaction path using the methods outlined in ref 41. The POLYRATE program[42] was used to calculate the rate coefficients.

In the chlorine reactions, the two spin−orbit (SO) states $^2P_{3/2}$ (lowest) and $^2P_{1/2}$ of Cl having degeneracies of 4 and 2, respectively, and separated by 882 cm^{-1} were included in the calculation of the electronic partition function. Similarly, in the OH reactions the $^2\Pi_{3/2}$ and $^2\Pi_{1/2}$ of the OH radical were included; both having a degeneracy equal to 2 and separated by 140 cm^{-1}. Spin−orbit coupling also has an effect on the barrier height of the reaction, which is not taken into account by the nonrelativistic ab initio calculations used here. Assuming that SO coupling is only relevant in the reactants region as found for the Cl + H_2 reaction[43,44] and the OH + H_2 reaction,[45] the effect is to lower the asymptotic potential energy of the reactants by 1/3 of the SO splitting in the Cl reactions (294 cm^{-1}) and 1/2 of the SO splitting in the OH reactions (70 cm^{-1}). This effect can be taken into account either by correcting the electronic partition function of the reactants as suggested by Manthe and co-workers[43,45] or increasing the energy all along the MEP except at the reactants. We have estimated the magnitude of the effect of SO coupling on the barrier height using the latter method because this may also affect the tunneling contribution.

The vibrational−rotational partition functions were assumed to be separable, and the rotational partition functions were approximated by their classical limit. The vibrational partition functions were calculated within the harmonic oscillator approximation for all modes (involving no scaling of the frequencies), except the C···H···OH torsional modes in the transition states of CH_4 + OH and CH_3Cl + OH, which were handled by the hindered rotor RW scheme.[46] The potentials of the torsional modes, $V(\phi)$, were calculated at the MP2/aug-cc-pVDZ level of theory and fitted to $V(\phi) = (1/2)W(1 - \cos 3\phi)$ for CH_4 + OH and $V(\phi) = (1/2)W(1 - \cos \phi)$ for CH_3Cl + OH; the barrier heights were found to be $W = 17$ and 303 cm^{-1}, respectively.

3. Results and Discussion

3.1. Experimental Study. The kinetic experiments were carried out under low NO_x conditions (NO_x < 100 ppbv). During the reaction of Cl atoms with chloromethane, OH radicals will eventually be generated from the HO_2 radicals and thereby influence the kinetics. We have previously modeled the degradation reactions of CH_3Cl in the static reactor using FACSIMILE[47] to find the optimum starting conditions, see Gola et al.[4] for a description of the model. Using 5 ppm CH_3Cl and 10−20 ppm Cl_2 as starting conditions, the model indicated that the loss of CH_3Cl because of reactions with OH radicals in the Cl atom experiments was less than 1‰ of the total loss. The model also predicted that the concentration of HC(O)Cl formed could be as high as 0.5 ppm; the absorption lines of this molecule could therefore interfere with the analyses of the C−H and C−D stretching regions of the spectrum. To prevent such a build-up, we employed the Philips TUV 30W lamp with $\lambda_{max} \approx 254$ nm, which will photolyze HC(O)Cl

$$HC(O)Cl + h\nu \rightarrow HCO + Cl \quad (3a)$$

$$\rightarrow CO + HCl \quad (3b)$$

The formation of HC(O)Cl can, in principle, also affect the kinetic study of the CH_3Cl reaction with OH because Cl atoms are released in the degradation of HC(O)Cl. The FACSIMILE model indicated that the loss of CH_3Cl in the OH radical experiments due to reactions with Cl atoms is at most 1‰ because the Cl atoms are scavenged effectively by the presence of 2×10^3 ppm H_2 in the reaction chamber.

Examples of the FTIR spectra obtained from the kinetic studies of the CH_3Cl/CH_2DCl and CH_3Cl/CHD_2Cl reactions with Cl atoms and the resulting residuals from the nonlinear least squares spectral analyses are shown in Figures 1a and S2a

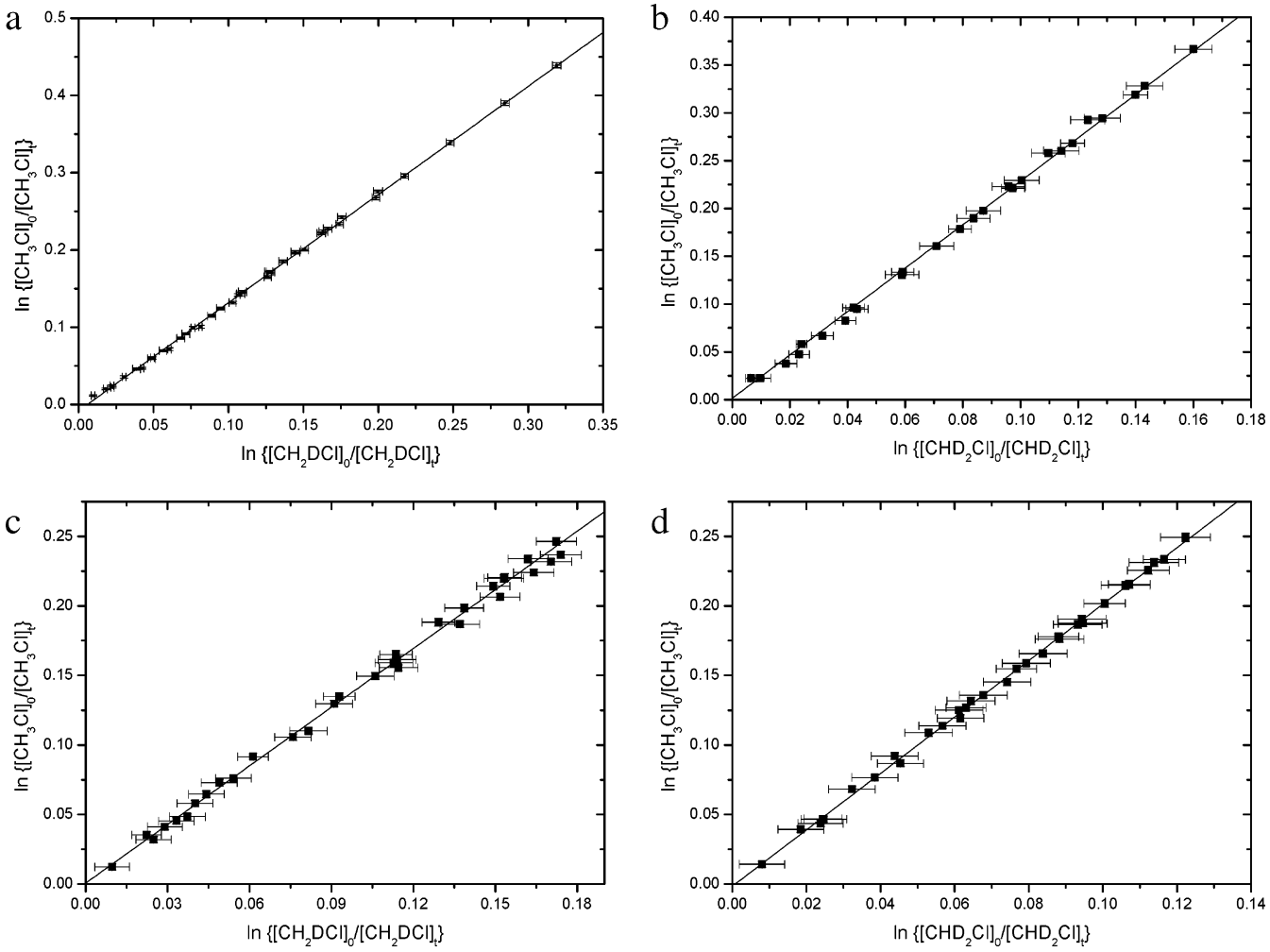

Figure 2. Relative rate plots showing the decays of CH_3Cl, CH_2DCl, and CHD_2Cl at 1013 hPa and 298 K in the presence of Cl atoms and OH radicals. The slopes correspond to the relative reaction rate $\alpha = k_{light}/k_{heavy}$; the errors on the slopes correspond to 2σ from the statistical analyses and do not include possible systematic errors. Error bars assigned to the individual data points correspond to 1σ from the spectral analyses that were carried out in the C−H stretching region. (a) Decay of CH_3Cl vs CH_2DCl in the presence of Cl atoms; $\alpha = 1.399 \pm 0.016$ (determined from 39 data points from four independent experiments). (b) Decay of CH_3Cl vs CHD_2Cl in the presence of Cl atoms; $\alpha = 2.27 \pm 0.04$ (26 data points from three independent experiments). (c) Decay of CH_3Cl vs CH_2DCl in the presence of OH radicals; $\alpha = 1.406 \pm 0.030$ (32 data points from four independent experiments). (d) Decay of CH_3Cl vs CHD_2Cl in the presence of OH radicals; $\alpha = 2.029 \pm 0.026$ (32 data points from four independent experiments).

(Supporting Information), respectively. The decays of CH_3Cl, CH_2DCl, and CHD_2Cl in the presence of Cl atoms are shown as plots of $\ln\{[CH_3Cl]_0/[CH_3Cl]_t\}$ versus $\ln\{[CH_2DCl]_0/[CH_2DCl]_t\}$ and $\ln\{[CH_3Cl]_0/[CH_3Cl]_t\}$ versus $\ln\{[CHD_2Cl]_0/[CHD_2Cl]_t\}$ in Figure 2a and b, respectively. Least-squares fitting of the data resulted in the following kinetic isotope effects: $k_{Cl+CH3Cl}/k_{Cl+CH2DCl} = 1.399 \pm 0.016$ and $k_{Cl+CH3Cl}/k_{Cl+CHD2Cl} = 2.27 \pm 0.04$ based on analyses of the C−H stretching region. The uncertainties represent 2σ from the statistical analyses and do not include possible systematic errors. Analyses of the C−D stretching regions of CH_2DCl and CHD_2Cl gave $k_{Cl+CH3Cl}/k_{Cl+CH2DCl} = 1.436 \pm 0.021$ and $k_{Cl+CH3Cl}/k_{Cl+CHD2Cl} = 2.273 \pm 0.030$, which, within the statistical uncertainties, are indistinguishable from the KIEs based on analysis of the C−H stretching region. We therefore cite the average of the two determinations together with error limits, which compass the extremes of the individual determinations, and report $k_{Cl+CH3Cl}/k_{Cl+CH2DCl} = 1.42 \pm 0.04$ and $k_{Cl+CH3Cl}/k_{Cl+CHD2Cl} = 2.27 \pm 0.04$. A spectrum of a yet unidentified compound with a *B*-type absorption band centered at 2270 cm^{-1} was included in the analyses of the C−D stretching region of both CH_2DCl and CHD_2Cl. The spectrum was generated in a separate experiment.

Figures 1b and S2b (Supporting Information) show experimental FTIR spectra of reaction mixtures $CH_3Cl/CH_2DCl/O_3/H_2$ and $CH_3Cl/CHD_2Cl/O_3/H_2$, respectively. As can be seen, the ozone band at 3046 cm^{-1} ($3\nu_3$) partly obscures the perpendicular bands of CH_3Cl (ν_4(E)) and CH_2DCl (ν_7(A″)) and overlaps the parallel bands of CH_3Cl (ν_1(E)), CH_2DCl (ν_1(A′)), and CHD_2Cl (ν_1(A′)). This complicated the spectral analysis substantially. The relative concentrations of CH_2DCl and CHD_2Cl during the reactions were determined from spectral analyses of the C−D stretching region (2280−2150 cm^{-1}) because this region is not obscured significantly. The spectrum of the unidentified compound mentioned above was included in the spectral analyses. The decay of CH_3Cl was determined from spectral analyses in the C−H stretching region in which the concentration of CH_2DCl/CHD_2Cl was fixed at the value determined in the C−D stretching region. From the decay data of the chloromethane isotopologues in the presence of OH radicals, shown in the form of $\ln\{[CH_3Cl]_0/[CH_3Cl]_t\}$ versus $\ln\{[CH_2DCl]_0/[CH_2DCl]_t\}$ and $\ln\{[CH_3Cl]_0/[CH_3Cl]_t\}$ versus $\ln\{[CHD_2Cl]_0/[CHD_2Cl]_t\}$ in Figure 2c and d, respectively, the following kinetic isotope effects were extracted: $k_{OH+CH3Cl}/k_{OH+CH2DCl} = 1.406 \pm 0.030$ and $k_{OH+CH3Cl}/k_{OH+CHD2Cl} = 2.029 \pm 0.026$. The uncertainties

represent 2σ from the least-squares analysis and refer to precision only. Because of the complicated spectral analysis, we increase the 2σ statistical uncertainty by 50%. We therefore report $k_{OH+CH3Cl}/k_{OH+CH2DCl} = 1.41 \pm 0.05$ and $k_{OH+CH3Cl}/k_{OH+CHD2Cl} = 2.03 \pm 0.05$.

The "natural" removal of CH_3Cl from the gas-phase (purified air) in the reactor is shown in Figure S3 (Supporting Information). Assuming the (small) decay to be of first order in CH_3Cl, the "natural" loss rate coefficient was determined to be 1.2×10^{-7} s^{-1} (lifetime $\approx$ 96 days). For a realistic reaction mixture in the OH radical experiments $CH_3Cl/H_2/O_3$ 5:2000:200 ppm in purified air, the loss rate coefficients of CH_3Cl and O_3 were determined simultaneously to be 5.6×10^{-7} and 1×10^{-6} s^{-1}, respectively. The lifetime of CH_3Cl in the reaction chamber under these conditions thus decreases to around 20 days. Assuming the difference between the two CH_3Cl loss rates to be due to gas-phase reaction with O_3 places an upper limit of $k_{O3+CH3Cl} < 10^{-22}$ cm^3 molecule^{-1} s^{-1}. The kinetic analysis according to eq 1 assumes that only one loss process is taking place; other loss processes such as gas-phase or surface reactions with the radical precursors, and "natural" wall loss will give rise to systematic errors in the kinetic isotope effects, especially in the OH reaction, which is slow. The OH experiments generally lasted for 5 h including spectral recording and waiting time between the photolysis, during which around 15% of the initial chloromethane reacted. Taking the rate coefficient for the OH reaction with chloromethane as 3.6×10^{-14} cm^3 molecule^{-1} s^{-1},[23] a rough estimate of the average OH concentration during the entire experiment (including waiting periods and time for spectrum recording) is 3×10^8 molecules cm^{-3}, which gives a ratio >20 between the loss due to reaction with OH radicals and the "dark" loss of chloromethane. Taking the numbers given above, a numerical simulation gives an estimate for the systematic error in $k_{OH+CH3Cl}/k_{OH+CH2DCl}$ of -0.014. For $k_{OH+CH3Cl}/k_{OH+CHD2Cl}$, the corresponding systematic error is estimated to be -0.034. That is, the known systematic errors in the OH radical experiments due to "dark" reactions of chloromethane result in apparent KIEs that are too small, but only by the same amount as the 2σ statistical error of the data analysis. For a realistic reaction mixture in the Cl atom experiments CH_3Cl/Cl_2 5:20 ppm in purified air, the loss rate coefficient of CH_3Cl was determined to be 3.7×10^{-7} s^{-1} (lifetime $\approx$ 31 days). The Cl atom experiments generally also lasted 5 h, the conversion of the chloromethanes, however, was around 30%. The recommended value of the CH_3Cl reaction-rate coefficient with Cl atoms at 298 K is 4.8×10^{-13} cm^3 molecule^{-1} s^{-1},[23] which places the average Cl atom concentration during the entire experiment around 4×10^7 atoms cm^{-3}, which gives a ratio >30 between the loss due to reaction with Cl atoms and the "dark" loss of chloromethane. The "dark" reactions will therefore not constitute an important systematic error in this system.

All available experimental kinetic isotope effects for the Cl and OH reactions of CH_4 and CH_3Cl are summarized in Table 1. The $^{12}C/^{13}C$ KIEs in the Cl and OH reactions of CH_3OH determined recently by Feilberg et al.[48] have been included for comparison. As can be seen, the $^{12}C/^{13}C$ KIE in the Cl reaction of CH_3OH is of similar magnitude as in CH_4 and CH_3Cl; for the OH reaction the $^{12}CH_3OH/^{13}CH_3OH$ KIE is of similar magnitude as for CH_3Cl, but, again, an order of magnitude larger than for CH_4.

3.2. Computational Study. *3.2.1. Structures and Energetics of Stationary Points.* The saddle point structures of the Cl and OH reactions of CH_4 and CH_3Cl were optimized at the MP2/aug-cc-pVDZ and MP2/aug-cc-pVTZ levels and are displayed in Figure 3. The structural results indicate that the aug-cc-pVDZ basis provides a reasonable description of these transition states when compared to the larger aug-cc-pVTZ basis; the largest difference is 2.2 pm, which is within what is expected for the two levels.[49] The saddle point structures of the Cl reactions with CH_4 and CH_3Cl were also optimized at the CCSD/aug-cc-pVDZ level to test the quality of the MP2 model, the CCSD model being more robust.[49] As can be seen from Figure 3a and c, the CCSD model predicts the saddle points of both systems to be more product-like than what is predicted by the MP2 model. It is difficult to estimate the full effect of this because CCSD calculations are currently too time-consuming to offer a realistic alternative in computations of the potential energy surfaces (PES) of the reactions investigated in this work.

The saddle point structure of the $CH_4 + Cl$ reaction from the present study agrees reasonably well with those from previous calculations.[15,19−21,50] In the $CH_4 + OH$ reaction, the computational levels used here predict a staggered conformation of the saddle point, while both staggered and eclipsed conformations have been reported in the literature.[11,16,18] This is not surprising because the OH group of the saddle point has a low barrier toward rotation (17 cm^{-1} at the MP2/aug-cc-pVDZ level of theory). We note that an eclipsed conformation was obtained for the saddle point structure when using the cc-pVDZ and cc-pVTZ basis sets, that is, when not including diffuse basis functions. The structure of the saddle point of the $CH_3Cl + Cl$ reaction from this work is more reactant-like than the structures reported previously,[9,12,13] especially when compared to the DFT results of Xiao et al.[12] For the $CH_3Cl + OH$ reaction, our saddle point structure agrees well with the one reported by Louis et al.,[10] but the structure presented by El-Taher[11] is much more

TABLE 1: Experimental ^{13}C and ^{2}H (D) Kinetic Isotope Effects, $\alpha = k_{Light}/k_{Heavy}$, in the Reactions of CH_4, CH_3Cl, and CH_3OH with Cl Atoms and OH Radicals at 298 K

	kinetic isotope effect	
isotopologues	Cl reaction	OH reaction
$CH_4/^{13}CH_4$	1.058 ± 0.002[8]	1.0039 ± 0.0004[7]
	1.0621 ± 0.0001[60]	
	1.066 ± 0.002[61,62]	
CH_4/CH_3D	1.459 ± 0.006[8]	1.25 ± 0.14[66]
	1.40 ± 0.13[54]	1.16 ± 0.07[67,a]
	1.36 ± 0.04[63]	1.13 ± 0.07[67,b]
	1.474 ± 0.02060	
	1.54 ± 0.05[64]	
	1.518 ± 0.041[65]	
CH_4/CH_2D_2	2.43 ± 0.01[8]	1.81 ± 0.28[66]
	2.17 ± 0.28[54]	
	2.19 ± 0.11[63]	
	2.38 ± 0.0564	
CH_4/CHD_3	4.73 ± 0.04[8]	3.30 ± 0.50[66]
	3.7 ± 0.6[54]	
	4.31 ± 0.09[63]	
	5.26 ± 0.364	
CH_4/CD_4	14.7 ± 0.2[8]	7.36 ± 0.88[66]
	12 ± 3[54]	6.55 ± 0.83[71,c]
	16.4 ± 1.3[63]	
	18.52 ± 0.4[64]	
	12 ± 2.0[68]	
	13.6 ± 1.0[69]	
	11 ± 1.0[70]	
$CH_3Cl/^{13}CH_3Cl$	1.070 ± 0.010[4]	1.059 ± 0.008[4]
CH_3Cl/CH_2DCl	1.42 ± 0.04[d]	1.41 ± 0.05[d]
CH_3Cl/CHD_2Cl	2.27 ± 0.04[d]	2.03 ± 0.05[d]
CH_3Cl/CD_3Cl	4.91 ± 0.07[4]	3.9 ± 0.4[4]
$CH_3OH/^{13}CH_3OH$	1.06 ± 0.01[48]	1.032 ± 0.006[48]

[a] Measured relative to HFC-134a. [b] Measured relative to HFC-141b. [c] Experimental value at 293 K was scaled to 298 K. [d] This work.

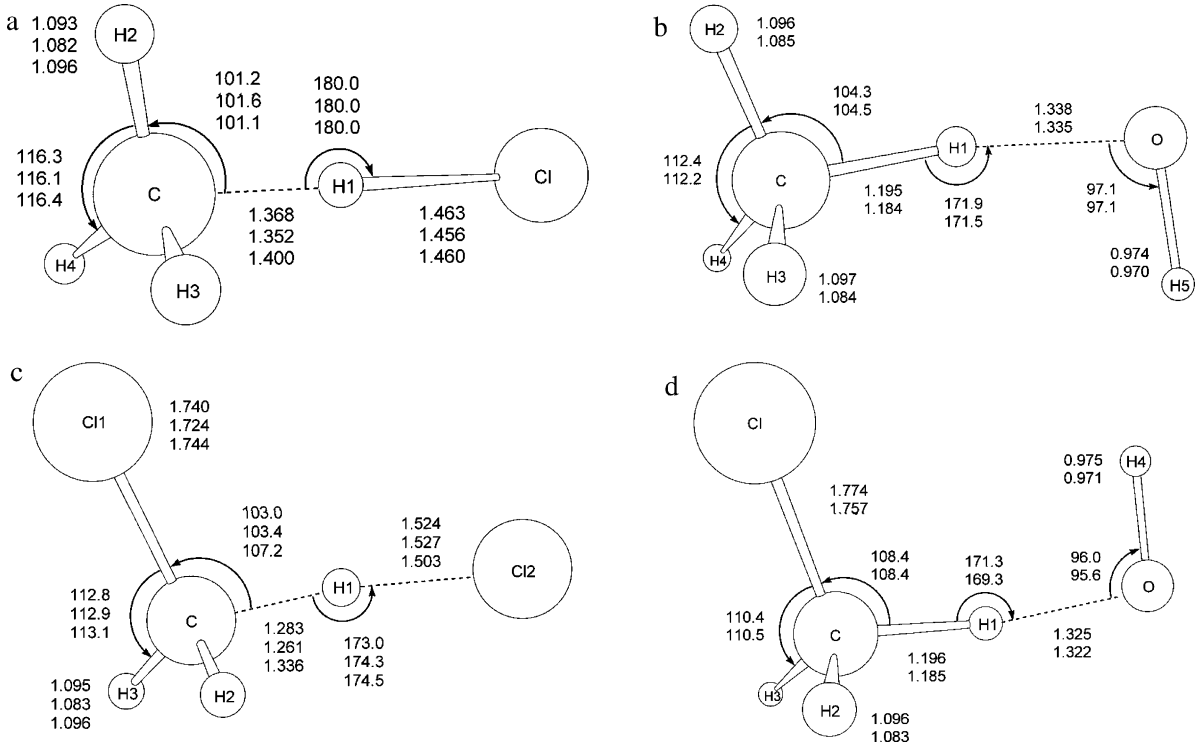

Figure 3. Geometrical parameters of the saddle points of the reactions (a) $CH_4 + Cl \rightarrow CH_3 + HCl$, (b) $CH_4 + OH \rightarrow CH_3 + H_2O$, (c) $CH_3Cl + Cl \rightarrow CH_2Cl + HCl$, and (d) $CH_3Cl + OH \rightarrow CH_2Cl + H_2O$ calculated at the MP2/aug-cc-pVDZ (top values), MP2/aug-cc-pVTZ, and CCSD/aug-cc-pVDZ (bottom values) levels of theory, respectively (only the saddle points of the Cl reactions of CH_4 and CH_3Cl have been optimized at the CCSD/aug-cc-pVDZ level). Bond lengths are in angstroms, and bond angles are in degrees.

product-like. However, the latter structure was obtained at a low computational level.

We have located a postreaction van der Waals adduct between CH_3 and HCl, Figure 4a, on the MEP of the Cl reaction with methane, which also has been reported by Chen et al.[50] and Yu and Nyman.[21] We note that the analytical potential energy surfaces of Roberto-Neto et al.[20] and Corchado et al.[19] do not include this adduct. A postreaction van der Waals adduct between CH_2Cl and HCl was also localized on the MEP of the Cl reaction with CH_3Cl, Figure 4b. This adduct was neither reported by Rayez et al.[9] nor by Xiao et al.[12] Our calculations confirm the existence of a cyclic hydrogen bonded prereaction adduct between CH_3Cl and the OH radical, Figure 4c, which was reported previously by El-Taher.[11] Chandra and Uchimaru[14] did not take this adduct into account in their study. As can be seen from the adduct structures in Figure 4, the intermolecular distances are 3−5 pm shorter when using the aug-cc-pVTZ basis than when using the smaller aug-cc-pVDZ basis. However, the potentials are expected to be relatively flat as the intermolecular distances become longer than 2 Å.

The energetics of the stationary points involved in the Cl and OH reactions of CH_4 and CH_3Cl are summarized and compared to previous results in Tables S1−S4 (Supporting Information); the agreement with literature data is generally good. Note, however, that the reported energies from this work do not include the effect of spin−orbit coupling on the reaction barrier height (Section 2.5). The calculated enthalpies of reaction for the OH and Cl reactions of CH_4 and CH_3Cl are in reasonable agreement with the experimental values with a discrepancy of at most 7 kJ mol^{-1} (Table S5, Supporting Information). The difference between the CCSD(T)/aug-cc-pVTZ//MP2/aug-cc-pVDZ and the CCSD(T)/EB//aug-cc-pVDZ energies are less than 1 kJ mol^{-1} for all systems except for the $Cl + CH_3Cl$ reaction where slightly larger differences are encountered (Table S3, Supporting Information). To test the sensitivity of the employed models with respect to structure, we also calculated the $Cl + CH_4$ reaction energies at the CCSD(T)/EB//MP2/aug-cc-pVTZ level of theory. As is seen from Table S1 (Supporting Information), the difference between the CCSD(T)/EB//MP2/aug-cc-pVDZ and the CCSD(T)/EB//MP2/aug-cc-pVTZ levels is at most 0.7 kJ mol^{-1}, again suggesting that the MP2/aug-cc-pVDZ level of theory describes the reaction systems reasonably well when compared to the MP2/aug-cc-pVTZ level.

For the loosely bound reaction adducts, one might expect the basis set superposition error (BSSE) to be significant. To estimate the magnitude of this effect, the BSSE in the CCSD(T)/EB//MP2/aug-cc-pVDZ model of the postreaction adduct in the chlorine reaction of methane was approximated by the counterpoise correction.[51] The BSSE was found to be around 0.5 kJ mol^{-1}, which we consider negligible in the present context.

3.2.2. Absolute Rate Coefficients. Figure 5a shows the potential energy of the minimum energy path, V_{MEP}, and the ground state vibrationally adiabatic potential energy curve, ΔV_a^G, as a function of the reaction coordinate for the $CH_4 + Cl$ reaction (the effect of spin−orbit coupling on the barrier height has not been included). The generalized normal-mode frequencies of the system as a function of the reaction coordinate are shown in Figure 5b. The two curves result from an interpolation to 150 ab initio points with gradients and where the Hessians have been computed at 50 of those points. The ΔV_a^G curve shows two maxima with a deep minimum between, which is in agreement with the analytic potential energy of Corchado et al.[19] At 0 K, the dynamical bottleneck is located at +0.28 bohr but shifts to −0.37 bohr at approximately 539 K. For the analytic PES of Corchado and co-workers, the shift in the location of the bottleneck takes place at 967 K. At the temperatures where the location of the generalized transition state changes suddenly,

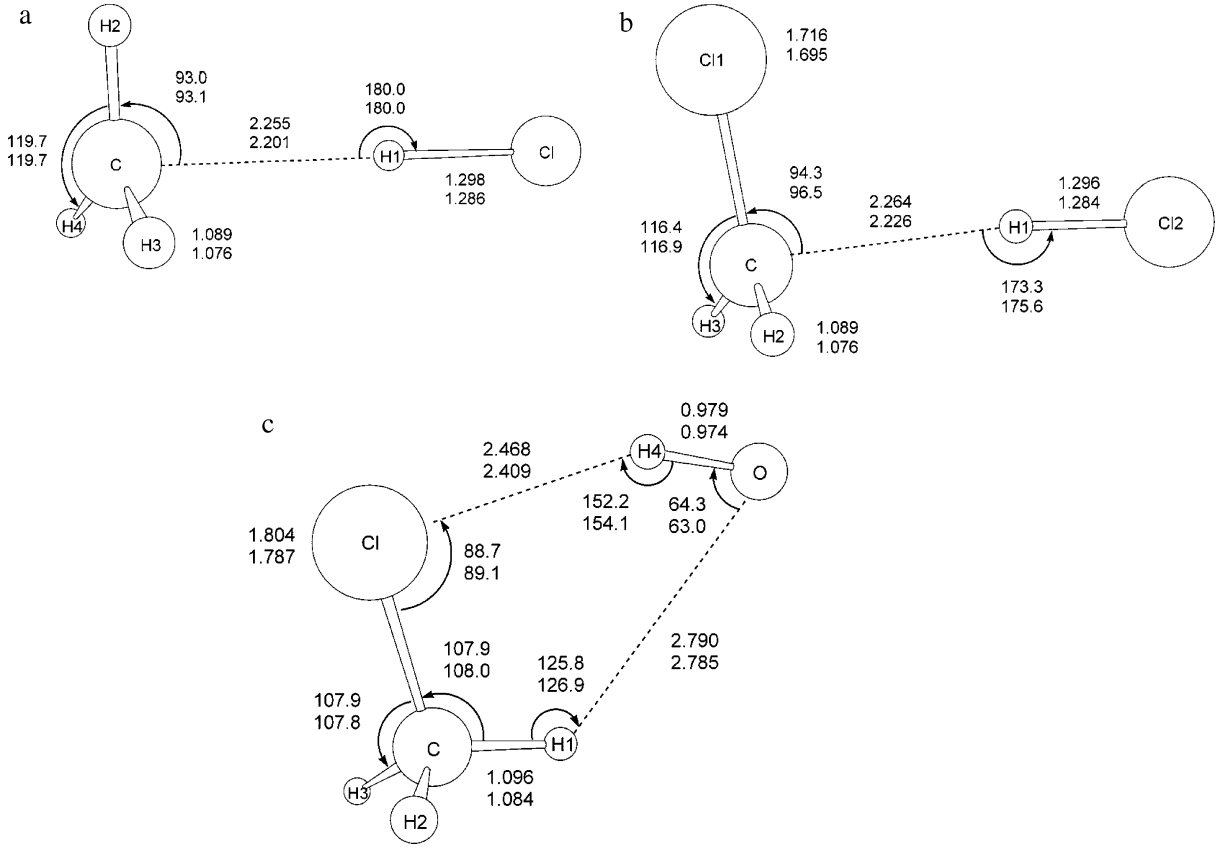

Figure 4. Geometrical parameters of (a) van der Waals adduct between CH_3 and HCl in the Cl reaction of CH_4, (b) van der Waals adduct between CH_2Cl and HCl in the Cl reaction of CH_3Cl, and (c) hydrogen bonded adduct between CH_3Cl and OH in the OH reaction of CH_3Cl calculated at the MP2/aug-cc-pVDZ (top values) and MP2/aug-cc-pVTZ (bottom values) levels, respectively (bond lengths in angstroms and bond angles in degrees).

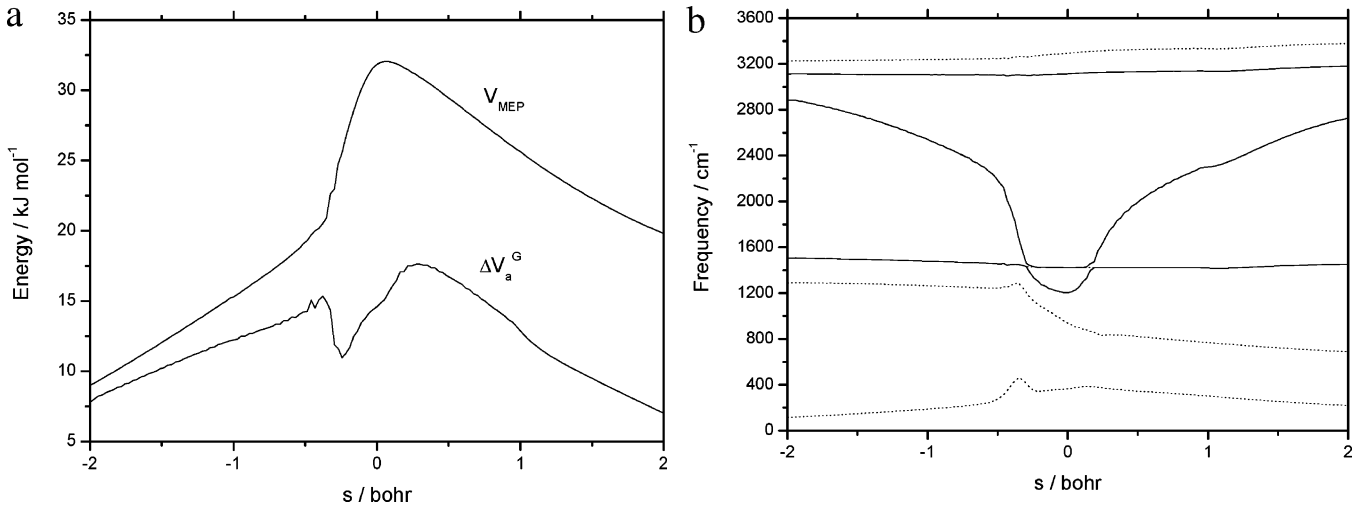

Figure 5. (a) Minimum energy path, V_{MEP} , and vibrationally adiabatic ground-state potential energy curve, ΔV_a^G, as a function of the reaction coordinate, *s*, for the reaction $CH_4 + Cl \rightarrow CH_3 + HCl$. All quantities are with respect to the reactants. The contribution from spin−orbit coupling has not been included. (b) Generalized normal-mode vibrational frequencies as a function of the reaction coordinate, *s*, for the reaction $CH_4 + Cl \rightarrow CH_3 + HCl$. Degenerate modes are dotted curves, and nondegenerate modes are solid curves.

the assumption of one dividing surface does not hold and significant recrossing over the dividing surface is to be expected. To deal with this problem, we have used canonical unified statistical theory (CUS) in which the rate coefficient from canonical variational theory is multiplied with a recrossing factor.[37,38]

Figure 6 shows an Arrhenius plot of calculated and experimental rate coefficients for the Cl reaction with methane. We see that our CUS/SCT calculation significantly underestimates the rate coefficient for the reaction and does not reproduce the temperature dependence correctly at low temperatures. There are two reasons for this: First of all, if we look at Table S1 (Supporting Information) we see that although there is good agreement between the electronic energies for our PES and the analytic PES of Corchado and co-workers,[19] we overestimate the vibrationally adiabatic barrier height for the reaction. This is not surprising because the vibrational frequencies have been calculated within the harmonic oscillator approximation, which

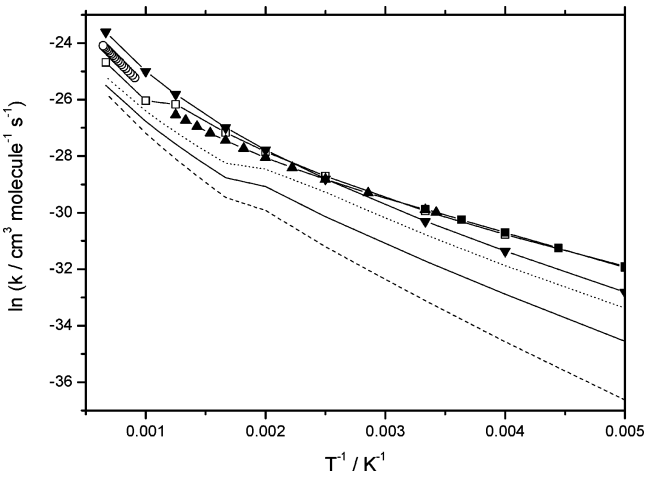

Figure 6. Arrhenius plot of calculated and experimental rate coefficients for the reaction $CH_4 + Cl \rightarrow CH_3 + HCl$. (—) This work, CUS/SCT with unscaled frequencies. (· · ·) This work, CUS/SCT with scaled vibrational frequencies (scaling factor = 0.959). (- - -) This work, CUS/SCT with contribution from spin−orbit coupling added. (−□−) Corchado et al.,[19] CUS/μOMT. (−▼−) Roberto-Neto et al.,[20] CVT/μOMT. (−■−) Atkinson et al.,[53] evaluation. (−▲−) Pilgrim et al.,[58] experiment. (−○−) Takahashi et al.,[59] experiment.

is known to overestimate the true frequencies. Scaling the Hessians by a factor of 0.959 (scaling factor taken from Computational Chemistry Comparison and Benchmark DataBase[52]) resulted in an increase of k_{Cl+CH4} from 1.6 to 4.1 × 10^{-14} cm^3 molecule^{-1} s^{-1} at 298 K with a modest change in the temperature dependency, see Figure 6. The experimental value is 1.0×10^{-13} cm^3 molecule^{-1} s^{-1}.[53] Second, the tunneling approximation we have used, the SCT model, underestimates the true tunneling probability, see later.

Figure S4a (Supporting Information) shows the V_{MEP} and the ΔV_a^G potential energy curves of the OH reaction of methane; the generalized normal-mode frequencies are shown in Figure S4b (Supporting Information). The vibrationally adiabatic potential curve has only one maximum, whereas the analytic PES of Espinosa-García and Corchado[17] shows two maxima with a shallow minimum between. Figure S5 (Supporting Information) shows an Arrhenius plot of calculated and experimental rate coefficients for the OH reaction of methane. Our calculation at the CVT/SCT level of theory underestimates the experimental rate coefficient at low temperatures.

The V_{MEP}, the ΔV_a^G potential energy curves, and the generalized normal-mode frequencies of the chlorine reaction of chloromethane are shown in Figure S6a and S6b, respectively (Supporting Information). The ΔV_a^G curve has two maxima: one at −0.30 bohr (global) and the other at +0.32 bohr with a shallow minimum between the two maxima at ca. +0.19 bohr. However, at all temperatures considered the energy difference between the second-highest maximum and the minimum is less than k_BT, k_B being the Boltzmann constant. Therefore, we have not used CUS for computing the rate coefficients in this case. The vibrationally adiabatic potential curve of Xiao and coworkers[12] also has two maxima, but the well they report between the two maxima is much deeper than the one we find. Our PES and that of Xiao and co-workers are therefore very different, the latter being much more product-like. Our calculation at the CVT/SCT level of theory predicts the rate coefficients to be less temperature-dependent than what has been predicted by Xiao and co-workers, see Figure S7 (Supporting Information).

The V_{MEP} and ΔV_a^G potential energy curves of the OH reaction with CH_3Cl are given in Figure S8a, and the generalized normal-mode frequencies are given in Figure S8b (Supporting Information). Our calculation underestimates the experimental rate coefficient at all temperatures, see Figure S9 (Supporting Information).

TABLE 2: $^{12}C/^{13}C$ Kinetic Isotope Effects in the Reaction $CH_4 + Cl \rightarrow CH_3 + HCl$[a]

	CUS/SCT[b]			
T/K	unscaled	scaled	CUS/μOMT[c]	experiment
200	1.077	1.027	1.216	
223	1.068	1.026		1.075 ± 0.005[d]
250	1.061	1.025	1.173	
298	1.050	1.024	1.141	1.058 ± 0.002[e]
350	1.042	1.023		
400	1.043	0.992	1.099	
500	1.035	1.045	1.074	
600	1.090	1.074	1.060	
700	1.081	1.071		
800	1.077	1.067	1.043	
1000	1.069	1.061	1.051	
1500	1.062	1.054	1.038	

[a] Abbreviations: CVT, canonical variational transition state theory; CUS, canonical unified statistical theory; SCT, small-curvature tunneling; μOMT, microcanonical optimized multidimensional tunneling. [b] This work with scaled and unscaled vibrational frequencies, scaling factor = 0.959. [c] Corchado et al.[19] [d] Saueressig et al.[62] [e] Feilberg et al.[8]

It is evident from Figures 6, S5, S7, and S9 (Supporting Information) that spin−orbit coupling has a significant effect on the absolute rate coefficients, especially in the Cl reactions. One may argue that the uncertainty in the ab initio calculations used in this work does not allow one to eliminate other sources of error of this magnitude, and it is likely that the effect of spin−orbit coupling partly cancels the incompleteness of the one-electron basis set and the treatment of electron correlation. However, we agree with Truhlar and co-workers[19,20] that the effect of spin−orbit coupling is systematic and therefore should be included, especially when electronic structure methods more sophisticated than those used in this work are being employed.

3.2.3. Kinetic Isotope Effects. The ^{13}C and ^{2}H kinetic isotope effects in the Cl reaction with methane are given in Tables 2 and 3. Our CUS/SCT calculations of KIE($^{12}CH_4/^{13}CH_4$) and KIE(CH_4/CH_3D) reproduce the experimental values well. For the kinetic isotope effects of CH_2D_2, CHD_3, and CD_4, the agreement with the experimental values systematically gets worse. The CUS/μOMT calculation of Corchado and coworkers[19] overestimates the ^{13}C KIE for this reaction. However, the use of the microcanonical optimized multidimensional tunneling approximation (μOMT) gives significantly better agreement with the experimental values for the deuterium kinetic isotope effects, although the calculation of Corchado and coworkers significantly overestimate the KIE(CH_4/CD_4) at 200 K compared to the recent experimental study of Sauer et al.[54]

To analyze the kinetic isotope effects in more detail, we performed a factor analysis as described in refs 19 and 55, but it was limited to investigations of the variational effect, the CUS effect, and the tunneling contribution only:

$$\mathrm{KIE} = \frac{k_{\mathrm{light}}}{k_{\mathrm{heavy}}} = \eta_{\mathrm{trans}}\eta_{\mathrm{rot}}\eta_{\mathrm{vib}}\eta_{\mathrm{tun}}\eta_{\mathrm{var}}\eta_{\mathrm{CUS}} \propto \eta_{\mathrm{tun}}\eta_{\mathrm{var}}\eta_{\mathrm{CUS}} \quad (4)$$

The tunneling contribution is given as $\eta_{tun} = \kappa^{SCT}(\mathrm{light})/\kappa^{SCT}(\mathrm{heavy})$, that is, the ratio of the tunneling factors for the light and the heavy isotopologue, the variational effect is given as $\eta_{var} = \mathrm{KIE}^{CVT}/\mathrm{KIE}^{TST}$, that is, the ratio of KIEs calculated using variational and conventional transition state theory, and η_{CUS}

TABLE 3: Kinetic Isotope Effects (KIEs) in the Reaction of CH_4, CH_3D, CH_2D_2, CHD_3, and CD_4 with Cl Atoms[a]

	KIE(CH_4/CH_3D)				KIE(CH_4/CH_2D_2)				KIE(CH_4/CHD_3)			KIE(CH_4/CD_4)			
	CUS/SCT[b]				CUS/SCT[b]				CUS/SCT[b]			CUS/SCT[b]			
T/K	unscaled	scaled	CUS /μOMT[c]	expt[d]	unscaled	scaled	CUS/ μOMT[c]	expt[d]	unscaled	scaled	expt[d]	unscaled	scaled	CUS/ μOMT[c]	expt[d]
200	1.43	1.26	2.61	1.54 ± 0.19	2.23	1.88	4.56	2.9 ± 0.5	4.27	4.05	5.6 ± 1.2	12.2	19.2	87.7	40 ± 15
250	1.37	1.32	2.20	1.45 ± 0.15	1.98	1.80	3.56	2.5 ± 0.4	3.34	3.39	4.4 ± 0.8	7.23	11.0	29.3	19 ± 6
298	1.32	1.37	1.93	1.40 ± 0.13	1.80	1.78	2.93	2.17 ± 0.28	2.77	2.83	3.7 ± 0.6	4.99	7.49	14.3	12 ± 3
350	1.27	1.43		1.36 ± 0.12	1.65	1.76		1.98 ± 0.24	2.18	2.50	3.3 ± 0.5	3.69	5.45		8.1 ± 2.2
400	1.20	1.44	1.58		1.49	1.71	2.16		2.00	2.25		2.43	4.18	5.6	
500	1.16	1.19	1.40		1.35	1.34	1.76		1.65	1.52		2.10	2.30	3.3	
600	1.02	1.00	1.29		0.78	1.01	1.53		0.91	0.93		1.08	1.00	2.4	
700	1.00	0.99			1.00	0.97			1.00	1.02		0.99	0.82		
800	0.98	0.98	1.16		0.97	0.97	1.29		0.95	0.97		1.95	2.18	1.6	
1000	1.11	1.14	0.95		1.25	1.30	0.87		1.40	1.50		1.57	1.70	0.8	
1500	1.05	1.07	1.09		1.10	1.12	1.19		1.16	1.21		1.22	1.27	1.4	

[a] Abbreviations: CVT, canonical variational transition state theory; CUS, canonical unified statistical theory; SCT, small-curvature tunneling; μOMT, microcanonical optimized multidimensional tunneling. [b] This work with scaled and unscaled vibrational frequencies, scaling factor = 0.959. [c] Corchado et al.[19] [d] Sauer et al.[54]

TABLE 4: $^{12}C/^{13}C$ Kinetic Isotope Effects in the Reaction $CH_4 + OH \rightarrow CH_3 + H_2O$[a]

	CVT/SCT[b]						
T/K	unscaled		scaled		CVT/SCT[c]	CUS/μOMT[d]	experiment[e]
200	1.014	(1.036)	1.023	(1.042)	1.0132	1.049	
250	1.005	(1.028)	1.010	(1.027)	1.0053	1.038	
298	1.003	(1.025)	1.010	(1.026)	1.0017	1.032[f]	1.0039 ± 0.0004
350	1.002	(1.024)	1.008	(1.022)	0.9997	1.029[g]	
400	1.001	(1.023)	1.007	(1.020)	0.9984	1.026	
500	0.997	(1.016)	1.093	(1.017)	0.9966	1.022	
600	0.998	(1.017)	1.004	(1.012)	0.9955	1.016	
700	0.999	(1.018)	1.006	(1.018)			
800	1.001	(1.020)	0.983	(1.009)		1.015	
1000	1.004	(1.021)	0.990	(1.006)	0.9931	1.013	
1500	1.000	(1.029)	0.994	(1.003)			

[a] Abbreviations: CVT, canonical variational transition state theory; CUS, canonical unified statistical theory; SCT, small-curvature tunneling; μOMT, microcanonical optimized multidimensional tunneling. [b] This work with scaled and unscaled vibrational frequencies and internal rotational mode treated as a hindered rotor, scaling factor = 0.959 (the numbers in parentheses are when the internal rotational mode is treated as a harmonic oscillator). [c] Lin et al.[18] (potential energy surface calculated at the MC3BB/MG3s level of theory). [d] Espinosa-Garcia and Corchado.[17] [e] Saueressig et al.[7] [f] 300 K. [g] 353 K.

$= KIE^{CUS}/KIE^{CVT}$, that is, the ratio of KIEs calculated using the CUS and CVT methods.

In the case of the CH_4 + Cl reaction, the factor analysis showed that the variational effect is dominating the $^{12}C/^{13}C$ KIE at low to moderate temperatures, $\eta_{var}(298\ K) = 1.05$ (see Table S6, Supporting Information). Above 539 K, the CUS effect is dominating. In contrast to our findings, tunneling was the single most important factor for the $^{12}C/^{13}C$ KIE for the analytical PES of Corchado et al.[19] A large variational effect for the CH_4/CD_4 KIE is found both in the present study, $\eta_{var}(298\ K) = 0.57$ (Table S6, Supporting Information) and in the work of Corchado and co-workers. However, a significantly larger contribution from tunneling was found in the work of Corchado et al.[19] Obviously, the small curvature tunneling approximation used in the present study is not able to describe the tunneling properly; the "corner cutting effect" for this reaction takes place over a larger part of the reaction swath than the SCT approximation is able to describe.[37,39,56] A more sophisticated tunneling method, for example, the large curvature tunneling approximation (LCT)[37] or the μOMT[37] approximation, is needed to describe these effects properly.

Table 4 gives the $^{12}C/^{13}C$ KIEs in the OH reaction of CH_4. We present two sets of calculations for the $^{12}C/^{13}C$ KIE; the values enclosed in parentheses are the kinetic isotope effects when all normal modes of vibration have been treated as harmonic oscillators, the other values are the isotope effects when the internal C···H···OH torsional mode was treated as a hindered rotor. Similar to what was found by Lin et al.,[18] the hindered rotor treatment of the mode is essential for getting the correct order of magnitude for the $^{12}C/^{13}C$ KIE in the OH reaction of CH_4. The temperature dependency of the $^{12}C/^{13}C$ KIE predicted in the present work is essentially the same as that predicted by Lin and co-workers.

The kinetic isotope effects in the OH reactions of CH_3D, CH_2D_2, CHD_3, and CD_4 are given in Table 5 (the internal C···H···OH torsional mode was treated as a hindered rotor). The variational effect is large ($\eta_{var}(298\ K) = 0.25$) for the CH_4/CD_4 KIE, see Table S7 (Supporting Information). As discussed above, the tunneling contribution is significantly underestimated.

The ^{13}C and ^{2}H KIEs in the Cl and OH reactions of CH_3Cl are given in Tables 6 and 7, respectively. A comparison between the $^{12}C/^{13}C$ KIEs in the Cl reactions with CH_4 and CH_3Cl, Tables 2 and 6, respectively, reveals that our calculations predict similar magnitudes of the $^{12}C/^{13}C$ KIEs for the Cl reactions with CH_3Cl and CH_4, which is also observed. Our calculations also predict the correct trend for the deuterium effects in the chlorine reaction of methane (Table 3) and chloromethane (Table 6). Further, we see from Table 4 ($KIE(^{12}CH_4/^{13}CH_4)$) and Table 7 ($KIE(^{12}CH_3Cl/^{13}CH_3Cl)$) that our calculations are in good agreement with the observed ^{13}C KIEs in the OH reactions of methane and chloromethane. The calculations are also in good agreement with the observed kinetic isotope effects of the OH reactions of CH_3Cl, CH_2DCl, and CHD_2Cl, but underestimate the experimental CH_3Cl/CD_3Cl kinetic isotope effect (Table 7).

TABLE 5: Kinetic Isotope Effects (KIEs) in the Reaction of CH_4, CH_3D, CH_2D_2, CHD_3, and CD_4 with OH Radicals[a]

	KIE(CH_4/CH_3D)				KIE(CH_4/CH_2D_2)				KIE(CH_4/CHD_3)				KIE(CH_4/CD_4)			
	CVT/SCT[b]				CVT/SCT[b]				CVT/SCT[b]				CVT/SCT[b]			
T/K	unscaled	scaled	CUS/ μOMT[c]	expt[d]	unscaled	scaled	CUS/ μOMT[c]	expt[d]	unscaled	scaled	CUS/ μOMT[c]	expt[d]	unscaled	scaled	CUS/ μOMT[c]	expt[d]
200	1.12	1.21	1.30		1.72	2.02	1.65		2.28	2.90	3.55		2.78	3.98	9.79	
250	1.08	1.17	1.29		1.43	1.69	1.55		1.72	2.20	2.94		1.95	2.80	5.73	
298	1.06	1.14	1.27[e]	1.294 ± 0.018	1.30	1.53	1.53[e]	1.81 ± 0.28	1.48	1.89	2.48[e]	3.30 ± 0.50	1.62	2.30	4.15[e]	7.36 ± 0.88
350	1.04	1.12	1.24[f]		1.21	1.43	1.49[f]		1.34	1.69	2.12[f]		1.42	1.98	3.00[f]	
400	1.03	1.10	1.21		1.16	1.35	1.42		1.29	1.54	1.89		1.30	1.76	2.45	
500	1.00	1.16	1.14		1.03	1.25	1.29		1.14	1.40	1.55		1.15	1.49	1.81	
600	0.99	1.05	1.10		1.03	1.14	1.20		1.06	1.17	1.34		1.05	1.20	1.49	
700	0.97	1.03			1.00	1.10			1.00	1.09			0.98	1.09		
800	0.99	0.99	1.10		0.98	1.03	1.19		0.96	1.00	1.33		0.93	0.97	1.45	
1000	1.03	0.96	1.05		0.95	0.96	1.13		0.90	0.89	1.22		0.86	0.84	1.32	
1500	0.92	0.94	1.00		0.86	0.88	1.05		0.79	0.85	1.08		0.72	0.78	1.11	

[a] Abbreviations: CVT, canonical variational transition state theory; CUS, canonical unified statistical theory; SCT, small-curvature tunneling; μOMT, microcanonical optimized multidimensional tunneling. [b] This work with scaled and unscaled vibrational frequencies and internal rotational mode treated as a hindered rotor, scaling factor = 0.959. [c] Espinosa-Garcia and Corchado.[17] [d] Gierczak et al.[66] [e] 300 K. [f] 353 K.

TABLE 6: Kinetic Isotope Effects (KIEs) in the Reaction of CH_3Cl, $^{13}CH_3Cl$, CH_2DCl, CHD_2Cl, and CD_3Cl with Cl Atoms[a]

	KIE($^{12}CH_3Cl/^{13}CH_3Cl$)			KIE(CH_3Cl/CH_2DCl)			KIE(CH_3Cl/CHD_2Cl)			KIE(CH_3Cl/CD_3Cl)		
	CVT/SCT[b]			CVT/SCT[b]			CVT/SCT[b]			CVT/SCT[b]		
T/K	unscaled	scaled	expt[c]	unscaled	scaled	expt[b]	unscaled	scaled	expt[b]	unscaled	scaled	expt[c]
200	1.195	1.021		2.17	2.18		2.89	4.32		10.1	15.1	
250	1.053	1.055		1.79	1.68		2.22	2.97		6.63	7.72	
298	1.035	1.037	1.070 ± 0.010	1.59	1.54	1.42 ± 0.04	1.95	2.51	2.27 ± 0.04	4.81	5.55	4.91 ± 0.07
350	1.030	1.030		1.46	1.45		1.51	2.20		3.76	4.26	
400	1.025	1.027		1.37	1.36		1.84	1.99		3.13	3.48	
500	1.014	1.015		1.23	1.30		1.54	1.71		2.39	2.61	
600	1.005	1.003		1.15	1.22		1.36	1.63		1.97	2.12	
700	0.999	1.000		1.09	1.17		1.24	1.49		1.70	1.83	
800	0.917	0.998		1.08	1.14		1.19	1.39		1.42	1.64	
1000	0.961	1.009		1.03	1.08		1.05	1.28		1.30	1.42	
1500	1.027	1.018		0.98	1.05		1.00	1.17		1.19	1.21	

[a] Abbreviations: CVT, canonical variational transition state theory; SCT, small-curvature tunneling. [b] This work with scaled and unscaled vibrational frequencies, scaling factor = 0.959. [c] Gola et al.[4]

TABLE 7: Kinetic Isotope Effects (KIEs) in the Reaction of CH_3Cl, $^{13}CH_3Cl$, CH_2DCl, CHD_2Cl, and CD_3Cl with OH Radicals[a]

	KIE($^{12}CH_3Cl/^{13}CH_3Cl$)			KIE(CH_3Cl/CH_2DCl)			KIE(CH_3Cl/CHD_2Cl)			KIE(CH_3Cl/CD_3Cl)		
	CVT/SCT[b]			CVT/SCT[b]			CVT/SCT[b]			CVT/SCT[b]		
T/K	unscaled	scaled	expt[c]	unscaled	scaled	expt[b]	unscaled	scaled	expt[b]	unscaled	scaled	expt[c]
200	1.070	1.076		1.54	1.64		2.26	2.78		3.41	4.67	
250	1.053	1.057		1.41	1.54		1.91	2.28		2.56	3.35	
298	1.044	1.047	1.059 ± 0.008	1.33	1.43	1.41 ± 0.05	1.72	2.00	2.03 ± 0.05	2.18	2.74	3.9 ± 0.4
350	1.040	1.042		1.28	1.37		1.60	1.82		1.96	2.37	
400	1.036	1.038		1.22	1.32		1.34	1.69		1.60	2.14	
500	1.032	1.033		1.16	1.23		1.30	1.44		1.43	1.65	
600	1.029	1.031		1.13	1.19		1.23	1.34		1.33	1.49	
700	1.028	1.031		1.10	1.16		1.19	1.27		1.26	1.38	
800	1.028	1.029		1.09	1.13		1.15	1.23		1.21	1.30	
1000	1.025	1.037		1.06	1.11		1.10	1.17		1.13	1.21	
1500	1.023	1.016		1.03	1.05		1.05	1.07		1.05	1.07	

[a] Abbreviations: CVT, for canonical variational transition state theory; SCT, small-curvature tunneling. [b] This work with scaled and unscaled vibrational frequencies and internal rotational mode treated as a harmonic oscillator, scaling factor = 0.959. [c] Gola et al.[4]

In the chlorine reaction with chloromethane, the variational effect is most important for the $^{12}C/^{13}C$ KIE with a factor of 1.06 at 298 K, Table S8 (Supporting Information). The variational effect is also the single largest effect for the CH_3Cl/CD_3Cl KIE, $\eta_{var}(298\ K) = 0.41$ (Table S8, Supporting Information). The variational effect and the tunneling contribution are of similar magnitude for the $^{12}C/^{13}C$ KIE in the OH reaction of CH_3Cl at room temperature; however, tunneling dominates at 200 K. The variational effect is very large ($\eta_{var}(298\ K) = 0.25$) for the kinetic isotope effect in the OH reactions of CH_3Cl and CD_3Cl, see Table S9 (Supporting Information). We note that although the characterized reaction adducts have an effect on the absolute rate coefficients of methane and chloromethane, they are of little importance for the kinetic isotope effects, at least at the theoretical level used in this work.

The effect of mechanical anharmonicities on the ^{13}C and ^{2}H KIEs in the Cl and OH reactions of CH_4 and CH_3Cl may be probed by scaling the Hessians (see section 3.2.2). The effect of this scaling on the $^{12}C/^{13}C$ KIEs was a small reduction by at most 3%, while the kinetic isotope effects for the deuterated species increased by 10−50% (there are some exceptions, however), see Tables 2−7 for details. Admittedly, this is a very

crude way of incorporating anharmonicities and care should be exercised in the interpretation of the results. However, the results show that anharmonicity may have a significant effect on the kinetic isotope effects.

The effect of spin−orbit coupling on the ^{13}C and ^{2}H KIEs in the Cl and OH reactions of CH_4 and CH_3Cl was found to be insignificant at all temperatures. However, the spin−orbit coupling effect was incorporated by increasing the energy all along the MEP except at the reactants. Consequently, the two isotopologues will be affected similarly. This may change when the geometry dependence of the spin−orbit effect is known for these reaction systems.

4. Conclusions

The present work suggests that the order of magnitude difference in the $^{12}C/^{13}C$ KIEs of the OH reaction with methane and chloromethane is due to the difference in barrier height of the C···H···OH torsional mode. In the transition state of the OH reaction with CH_4, the torsional barrier is only 17 cm^{-1} at the MP2/aug-cc-pVDZ level. Therefore, it cannot be treated as a harmonic oscillator. The barrier of the corresponding mode in the TS of the OH reaction with CH_3Cl is 303 cm^{-1}. The hindered rotor scheme we have used is the same as that used by Lin et al.,[18] and as was stated by Lin and co-workers, the internal rotational axis in this scheme goes through the center of mass of the whole system instead of through the axis connecting the carbon and the oxygen atom. Therefore, the internal rotational mode contributes to the $^{12}C/^{13}C$ kinetic isotope effect.

As seen in Table 1, the $^{12}C/^{13}C$ KIE in the OH reaction of CH_3OH is also an order of magnitude larger than that for CH_4. By judging from the TS structure of CH_3OH + OH reported by Jodkowski et al.[57] (Figure 1 in their paper), it is likely that the same situation for the $^{12}C/^{13}C$ KIE in the OH reaction of CH_3Cl compared to CH_4 also holds for CH_3OH.

On the basis of the results from this work and the studies of Truhlar and co-workers,[19,20] the deuterium kinetic isotope effects in the Cl reactions of CH_4 and CH_3Cl can be explained by variational effects and tunneling. Our calculations are not able to reproduce the observed trend for the deuterium KIEs in the OH reactions of CH_4 and CH_3Cl. However, as we have pointed out already, the tunneling method used in this work (SCT) is not able to describe the tunneling effect properly. This is seen clearly for the perdeuterated species. We suggest that the use of a more sophisticated tunneling method will result in better agreement with the experimental observations for the deuterium KIEs in the OH reactions of methane and chloromethane.

Acknowledgment. This work is part of the ACTION project supported by the Norwegian Research Council under contract 160272/V30. The Norwegian High Performance Computing Consortium is acknowledged for grants of computing time. Professor Donald G. Truhlar is acknowledged for providing the POLYRATE program. S.R.S. acknowledges a researcher mobility grant from the Nordic Network for Chemical Kinetics supported by the Nordic Academy for Advanced study (NorFA). We thank Dr. Matthew S. Johnson (Copenhagen) for his valuable assistance in recording the high-resolution spectra of the chloromethane isotopologues. Professor Trygve Helgaker and Dr. Lihn Bache-Andreassen at the University of Oslo are acknowledged for helpful discussions.

Supporting Information Available: Energetics of stationary points involved in the reactions CH_4 + Cl (Table S1), CH_4 + OH (Table S2), CH_3Cl + Cl (Table S3), and CH_3Cl + OH (Table S4). Enthalpies of reaction for the Cl and OH reactions of CH_4 and CH_3Cl (Table S5). Factor analysis of the kinetic isotope effects in the reactions CH_4 + Cl (Table S6), CH_4 + OH (Table S7), CH_3Cl + Cl (Table S8), and CH_3Cl + OH (Table S9). High-resolution FTIR spectra of CH_2DCl and CHD_2Cl (Figure S1a and b). Experimental FTIR spectra of the reaction mixtures $CH_3Cl/CHD_2Cl/Cl_2$ and $CH_3Cl/CHD_2Cl/O_3/H_2$ (Figure S2a and b). Decay curves for CH_3Cl and O_3 in the reactor as a function of time (Figure S3). Minimum energy paths, ground-state vibrationally adiabatic potential energy curves, and generalized normal-mode vibrational frequencies as a function of the reaction coordinate for the reactions CH_4 + OH (Figure S4a and b), CH_3Cl + Cl (Figure S6a and b), and CH_3Cl + OH (Figure S8a and b). Arrhenius plots of calculated and experimental rate coefficients for the reactions CH_4 + OH (Figure S5a and b), CH_3Cl + Cl (Figure S7a and b), and CH_3Cl + OH (Figure S9a and b). This material is available free of charge via the Internet at http://pubs.acs.org.

References and Notes

(1) (a) Khalil, M. A. K.; Rasmussen, R. A. *Atmos. Environ.* **1999**, *33*, 1305. (b) Keene, W. C.; Khalil, M. A. K.; Erickson, D. J., III.; McCulloch, A.; Graedel, T. E.; Lobert, J. M.; Aucott, M. L.; Gong, S. L.; Harper, D. B.; Kleiman, G.; Midgley, P.; Moore, R. M.; Seuzaret, C.; Sturges, W. T.; Benkovitz, C. M.; Koropalov, V.; Barrie, L. A.; Li, Y. F. *J. Geophys. Res.*, [*Atmos.*] **1999**, *104*, 8429.

(2) Montzka, S. A.; Fraser, P. J. Controlled Substances and Other Source Gases; WMO Scientific Assessment of Ozone Depletion, Global Ozone Research and Monitoring Project; Report No. 47; World Meteorological Organization, Geneva, 2003; http://www.wmo.ch/web/arep/reports/ozone_2002/06_chapter1.pdf.

(3) Hamilton, J. T. G.; McRoberts, W. C.; Keppler, F.; Kalin, R. M.; Harper, D. B. *Science* **2003**, *301*, 206.

(4) Gola, A. A.; D'Anna, B.; Feilberg, K. L.; Sellevåg, S. R.; Bache-Andreassen, L.; Nielsen, C. J. *Atmos. Chem. Phys.* **2005**, *5*, 2395.

(5) Keppler, F.; Kalin, R. M.; Harper, D. B.; McRoberts, W. C.; Hamilton, J. T. G. *Biogeosciences* **2004**, *1*, 123.

(6) Keppler, F.; Harper, D. B.; Röckmann, T.; Hamilton, J. T. G. *Atmos. Chem. Phys.* **2005**, *5*, 2403.

(7) Saueressig, G.; Crowley, J. N.; Bergamaschi, P.; Bruhl, C.; Brenninkmeijer, C. A. M.; Fischer, H. *J. Geophys. Res.*, [*Atmos.*] **2001**, *106*, 23127.

(8) Feilberg, K. L.; Griffith, D. W. T.; Johnson, M. S.; Nielsen, C. J. *Int. J. Chem. Kinet.* **2005**, *37*, 110.

(9) Rayez, M.-T.; Rayez, J.-C.; Sawerysyn, J.-P. *J. Phys. Chem.* **1994**, *98*, 11342.

(10) Louis, F.; Gonzalez, C. A.; Huie, R. E.; Kurylo, M. J. *J. Phys. Chem. A* **2000**, *104*, 8773.

(11) El-Taher, S. *Int. J. Quantum Chem.* **2001**, *84*, 426.

(12) Xiao, J.-F.; Li, Z.-S.; Ding, Y.-H.; Liu, J.-Y.; Huang, X.-R.; Sun, C.-C. *Phys. Chem. Chem. Phys.* **2001**, *3*, 3955.

(13) Murray, C.; Retail, B.; Orr-Ewing, A. J. *Chem. Phys.* **2004**, *301*, 239.

(14) Chandra, A. K.; Uchimaru, T. *J. Phys. Chem. A* **2000**, *104*, 8535.

(15) Truong, T. N.; Truhlar, D. G.; Baldridge, K. K.; Gordon, M. S.; Steckler, R. *J. Chem. Phys.* **1989**, *90*, 7137.

(16) (a) Truong, T. N.; Truhlar, D. G. *J. Chem. Phys.* **1990**, *93*, 1761. (b) Gonzalez, C.; McDouall, J. J. W.; Schlegel, H. B. *J. Phys. Chem.* **1990**, *94*, 7467. (c) Dobbs, K. D.; Dixon, D. A.; Komornicki, A. *J. Chem. Phys.* **1993**, *98*, 8852. (d) Skokov, S.; Wheeler, R. A. *Chem. Phys. Lett.* **1997**, *271*, 251. (e) Melissas, V. S.; Truhlar, D. G. *J. Chem. Phys.* **1993**, *99*, 3542. (f) Melissas, V. S.; Truhlar, D. G. *J. Chem. Phys.* **1993**, *99*, 1013. (g) Masgrau, L.; Gonzalez-Lafont, A.; Lluch, J. M. *J. Chem. Phys.* **2001**, *114*, 2154. (h) Masgrau, L.; Gonzalez-Lafont, A.; Lluch, J. M. *J. Chem. Phys.* **2001**, *115*, 4515.

(17) Espinosa-Garcia, J.; Corchado, J. C. *J. Chem. Phys.* **2000**, *112*, 5731.

(18) Lin, H.; Zhao, Y.; Ellingson, B. A.; Pu, J.; Truhlar, D. G. *J. Am. Chem. Soc.* **2005**, *127*, 2830.

(19) Corchado, J. C.; Truhlar, D. G.; Espinosa-Garcia, J. *J. Chem. Phys.* **2000**, *112*, 9375.

(20) Roberto-Neto, O.; Coitino, E. L.; Truhlar, D. G. *J. Phys. Chem. A* **1998**, *102*, 4568.

(21) Yu, H.-G.; Nyman, G. *J. Chem. Phys.* **1999**, *111*, 6693.

(22) Weiss, E.; Lambertsen, T.; Schubert, B.; Cockcroft, J. K. *J. Organomet. Chem.* **1988**, *358*, 1.

(23) Sander, S. P.; Friedl, R. R.; Golden, D. M.; Kurylo, M. J.; Huie, R. E.; Orkin, V. L.; Moortgat, G. K.; Ravishankara, A. R.; Kolb, C. E.; Molina, M. J.; Finlayson-Pitts, B. J. *Chemical Kinetics and Photochemical Data for Use in Atmospheric Studies. Evaluation Number 14*; National Aeronautics and Space Administration, Jet Propulsion Laboratory, California Institute of Technology: Pasadena, California, 2003.

(24) Griffith, D. W. T. *Appl. Spectrosc.* **1996**, *50*, 59.

(25) Rothman, L. S.; Jacquemart, D.; Barbe, A.; Benner, D. C.; Birk, M.; Brown, L. R.; Carleer, M. R.; Chackerian, C., Jr.; Chance, K.; Coudert, L. H.; Dana, V.; Devi, V. M.; Flaud, J.-M.; Gamache, R. R.; Goldman, A.; Hartmann, J.-M.; Jucks, K. W.; Maki, A. G.; Mandin, J.-Y.; Massie, S. T.; Orphal, J.; Perrin, A.; Rinsland, C. P.; Smith, M. A. H.; Tennyson, J.; Tolchenov, R. N.; Toth, R. A.; Auwera, J. V.; Varanasi, P.; Wagner, G. *J. Quant. Spectrosc. Radiat. Transfer* **2005**, *96*, 139.

(26) York, D. *Can. J. Phys.* **1966**, *44*, 1079.

(27) Møller, C.; Plesset, M. S. *Phys. Rev.* **1934**, *46*, 618.

(28) (a) Cizek, J. *Adv. Chem. Phys.* **1969**, *14*, 35. (b) Purvis, G. D., III.; Bartlett, R. J. *J. Chem. Phys.* **1982**, *76*, 1910. (c) Scuseria, G. E.; Janssen, C. L.; Schaefer, H. F., III. *J. Chem. Phys.* **1988**, *89*, 7382. (d) Scuseria, G. E.; Schaefer, H. F., III. *J. Chem. Phys.* **1989**, *90*, 3700.

(29) Raghavachari, K.; Trucks, G. W.; Pople, J. A.; Head-Gordon, M. *Chem. Phys. Lett.* **1989**, *157*, 479.

(30) Frisch, M. J.; Trucks, G. W.; Schlegel, H. B.; Scuseria, G. E.; Robb, M. A.; Cheeseman, J. R.; Montgomery, J. A., Jr.; Vreven, T.; Kudin, K. N.; Burant, J. C.; Millam, J. M.; Iyengar, S. S.; Tomasi, J.; Barone, V.; Mennucci, B.; Cossi, M.; Scalmani, G.; Rega, N.; Petersson, G. A.; Nakatsuji, H.; Hada, M.; Ehara, M.; Toyota, K.; Fukuda, R.; Hasegawa, J.; Ishida, M.; Nakajima, T.; Honda, Y.; Kitao, O.; Nakai, H.; Klene, M.; Li, X.; Knox, J. E.; Hratchian, H. P.; Cross, J. B.; Adamo, C.; Jaramillo, J.; Gomperts, R.; Stratmann, R. E.; Yazyev, O.; Austin, A. J.; Cammi, R.; Pomelli, C.; Ochterski, J. W.; Ayala, P. Y.; Morokuma, K.; Voth, G. A.; Salvador, P.; Dannenberg, J. J.; Zakrzewski, V. G.; Dapprich, S.; Daniels, A. D.; Strain, M. C.; Farkas, O.; Malick, D. K.; Rabuck, A. D.; Raghavachari, K.; Foresman, J. B.; Ortiz, J. V.; Cui, Q.; Baboul, A. G.; Clifford, S.; Cioslowski, J.; Stefanov, B. B.; Liu, G.; Liashenko, A.; Piskorz, P.; Komaromi, I.; Martin, R. L.; Fox, D. J.; Keith, T.; Al-Laham, M. A.; Peng, C. Y.; Nanayakkara, A.; Challacombe, M.; Gill, P. M. W.; Johnson, B.; Chen, W.; Wong, M. W.; Gonzalez, C.; Pople, J. A. *Gaussian 03, Revision B.03*; Gaussian, Inc.: Pittsburgh, PA, 2003.

(31) (a) Dunning, T. H., Jr. *J. Chem. Phys.* **1989**, *90*, 1007. (b) Kendall, R. A.; Dunning, T. H., Jr.; Harrison, R. J. *J. Chem. Phys.* **1992**, *96*, 6796.

(32) Halkier, A.; Helgaker, T.; Jorgensen, P.; Klopper, W.; Koch, H.; Olsen, J.; Wilson, A. K. *Chem. Phys. Lett.* **1998**, *286*, 243.

(33) (a) Gonzalez, C.; Schlegel, H. B. *J. Chem. Phys.* **1989**, *90*, 2154. (b) Gonzalez, C.; Schlegel, H. B. *J. Phys. Chem.* **1990**, *94*, 5523.

(34) Corchado, J. C.; Coitino, E. L.; Chuang, Y.-Y.; Fast, P. L.; Truhlar, D. G. *J. Phys. Chem. A* **1998**, *102*, 2424.

(35) Chuang, Y.-Y.; Corchado, J. C.; Truhlar, D. G. *J. Phys. Chem. A* **1999**, *103*, 1140.

(36) Garrett, B. C.; Truhlar, D. G. *J. Phys. Chem.* **1979**, *83*, 1052.

(37) Truhlar, D. G.; Isaacson, A. D.; Garrett, B. C. Generalized transition state theory. In *The Theory of Chemical Reaction Dynamics*; Baer, M., Ed.; CRC Press: Boca Raton, FL, 1985; Vol. 4; p 65.

(38) Garrett, B. C.; Truhlar, D. G. *J. Chem. Phys.* **1982**, *76*, 1853.

(39) Liu, Y.-P.; Lynch, G. C.; Truong, T. N.; Lu, D.-H.; Truhlar, D. C.; Garrett, B. C. *J. Am. Chem. Soc.* **1993**, *115*, 2408.

(40) Garrett, B. C.; Truhlar, D. G.; Grev, R. S.; Magnuson, A. W. *J. Phys. Chem.* **1980**, *84*, 1730.

(41) (a) Fast, P. L.; Corchado, J. C.; Truhlar, D. G. *J. Chem. Phys.* **1998**, *109*, 6237. (b) Gonzalez-Lafont, A.; Villa, J.; Lluch, J. M.; Bertran, J.; Steckler, R.; Truhlar, D. G. *J. Phys. Chem. A* **1998**, *102*, 3420. (c) Villa, J.; Corchado, J. C.; Gonzalez-Lafont, A.; Lluch, J. M.; Truhlar, D. G. *J. Phys. Chem. A* **1999**, *103*, 5061.

(42) Corchado, J. C.; Chuang, Y.-Y.; Fast, P. L.; Villà, J.; Hu, W.-P.; Liu, Y.-P.; Lynch, G. C.; Nguyen, K. A.; Jackels, C. F.; Melissas, V. S.; Lynch, B. J.; Rossi, I.; Coitiño, E. L.; Fernandez-Ramos, A.; Pu, J.; Albu, T. V.; Steckler, R.; Garrett, B. C.; Isaacson, A. D.; Truhlar, D. G. *POLYRATE*, version 9.3; University of Minnesota: Minneapolis, MN, 2002.

(43) Manthe, U.; Bian, W.; Werner, H. J. *Chem. Phys. Lett.* **1999**, *313*, 647.

(44) (a) Manthe, U.; Capecchi, G.; Werner, H.-J. *Phys. Chem. Chem. Phys.* **2004**, *6*, 5026. (b) Capecchi, G.; Werner, H.-J. *Phys. Chem. Chem. Phys.* **2004**, *6*, 4975.

(45) Matzkies, F.; Manthe, U. *J. Chem. Phys.* **1998**, *108*, 4828.

(46) Chuang, Y.-Y.; Truhlar, D. G. *J. Chem. Phys.* **2000**, *112*, 1221.

(47) FACSIMILE for Windows, Version 4.0.31; MCPA Software Ltd.

(48) Feilberg, K. L.; Johnson, M. S.; Nielsen, C. J. *J. Phys. Chem. A*, to be submitted, 2005.

(49) Helgaker, T.; Jørgensen, P.; Olsen, J. *Molecular Electronic-Structure Theory*; John Wiley & Sons Ltd: Chichester, U.K., 2000.

(50) Chen, Y.; Tschuikow-Roux, E.; Rauk, A. *J. Phys. Chem.* **1991**, *95*, 9832.

(51) (a) Boys, S. F.; Bernardi, F. *Mol. Phys.* **1970**, *19*, 553. (b) Simon, S.; Duran, M.; Dannenberg, J. J. *J. Chem. Phys.* **1996**, *105*, 11024.

(52) Computational Chemistry Comparison and Benchmark DataBase (CCCBDB), NIST Standard Reference Database 101; National Institute of Standards and Technology, 2005; http://srdata.nist.gov/cccbdb/.

(53) Atkinson, R.; Baulch, D. L.; Cox, R. A.; Crowley, J. N.; Hampson, R. F., Jr.; Hynes, R. G.; Jenkin, M. E.; Kerr, J. A.; Rossi, M. J.; Troe, J. Summary of evaluated kinetic and photochemical data for atmospheric chemistry; IUPAC Subcommittee on Gas Kinetic Data Evaluation for Atmospheric Chemistry, Web Version July 2004; http://www.iupac-kinetic.ch.cam.ac.uk/.

(54) Sauer, F.; Bauerle, S.; Burkholder, J. B.; Ravishankara, A. R. Temperature dependence of the Cl atom reaction with deuterated methanes; Faraday Discussion 130 Atmospheric Chemistry; 11−13 April 2005, University of Leeds, U.K.; Royal Society of Chemistry, 2005, pp P48.

(55) Joseph, T.; Steckler, R.; Truhlar, D. G. *J. Chem. Phys.* **1987**, *87*, 7036.

(56) Skodje, R. T.; Truhlar, D. G.; Garrett, B. C. *J. Phys. Chem.* **1981**, *85*, 3019.

(57) Jodkowski, J. T.; Rayez, M.-T.; Rayez, J.-C.; Berces, T.; Dobe, S. *J. Phys. Chem. A* **1999**, *103*, 3750.

(58) Pilgrim, J. S.; McIlroy, A.; Taatjes, C. A. *J. Phys. Chem. A* **1997**, *101*, 1873.

(59) Takahashi, K.; Yamamoto, O.; Inomata, T. *Proc. Comb. Inst.* **2002**, *29*, 2447.

(60) Tyler, S. C.; Ajie, H. O.; Rice, A. L.; Cicerone, R. J.; Tuazon, E. C. *Geophys. Res. Lett.* **2000**, *27*, 1715.

(61) Crowley, J. N.; Saueressig, G.; Bergamaschi, P.; Fischer, H.; Harris, G. W. *Chem. Phys. Lett.* **1999**, *303*, 268.

(62) Saueressig, G.; Bergamaschi, P.; Crowley, J. N.; Fischer, H.; Harris, G. W. *Geophys. Res. Lett.* **1995**, *22*, 1225.

(63) Wallington, T. J.; Hurley, M. D. *Chem. Phys. Lett.* **1992**, *189*, 437.

(64) Boone, G. D.; Agyin, F.; Robichaud, D. J.; Tao, F.-M.; Hewitt, S. A. *J. Phys. Chem. A* **2001**, *105*, 1456.

(65) Saueressig, G.; Bergamaschi, P.; Crowley, J. N.; Fischer, H.; Harris, G. W. *Geophys. Res. Lett.* **1996**, *23*, 3619.

(66) Gierczak, T.; Talukdar, R. K.; Herndon, S.; Vaghjiani, G. L.; Ravishankara, A. R. *J. Phys. Chem. A* **1997**, *101*, 3125.

(67) DeMore, W. B. *J. Phys. Chem.* **1993**, *97*, 8564.

(68) Matsumi, Y.; Izumi, K.; Skorokhodov, V.; Kawasaki, M.; Tanaka, N. *J. Phys. Chem. A* **1997**, *101*, 1216.

(69) Clyne, M. A. A.; Walker, R. F. *J. Chem. Soc., Faraday Trans. 1* **1973**, *69*, 1547.

(70) Chiltz, G.; Eckling, R.; Goldfinger, P.; Huybrechts, G.; Johnston, H. S.; Meyers, L.; Verbeke, G. *J. Chem. Phys.* **1963**, *38*, 1053.

(71) Dunlop, J. R.; Tully, F. P. *J. Phys. Chem.* **1993**, *97*, 11148.